



Article

The Effect of Substrate Biasing during DC Magnetron Sputtering on the Quality of VO₂ Thin Films and Their Insulator–Metal Transition Behavior

Chunzi Zhang ¹, Ozan Gunes ¹ , Yuanshi Li ², Xiaoyu Cui ³, Masoud Mohammadtaheri ², Shi-Jie Wen ⁴, Rick Wong ⁴, Qiaoqin Yang ² and Safa Kasap ^{1,*} 

¹ Department of Electrical and Computer Engineering, University of Saskatchewan, 57 Campus Drive, Saskatoon, SK S7N 5A9, Canada

² Department of Mechanical Engineering, University of Saskatchewan, 57 Campus Drive, Saskatoon, SK S7N 5A9, Canada

³ Canadian Light Source Inc., 44 Innovation Boulevard, Saskatoon, SK S7N 2V3, Canada

⁴ Cisco Systems Inc., San Jose, CA 95134, USA

* Correspondence: safa.kasap@usask.ca; Tel.: +1-306-966-5390

Received: 1 May 2019; Accepted: 28 June 2019; Published: 5 July 2019



Abstract: In this work, VO₂ thin films were deposited on Si wafers (onto (100) surface) by DC magnetron sputtering under different cathode bias voltages. The effects of substrate biasing on the structural and optical properties were investigated. The results show that the metal–insulator transition (MIT) temperature of VO₂ thin films can be increased up to 14 K by applying a cathode bias voltage, compared to deposition conditions without any bias. The decrease in the transition efficiency and increase in the transition temperature are attributed to the enlarged grain size, increased defects, and the residual stress in the VO₂ thin films induced by biasing. The optical transmittance measurements for different thickness films indicate an attenuation coefficient of $3.1 \times 10^7 \text{ m}^{-1}$ at 2000 nm or an extinction coefficient of 4.9 in the metal phase. The optical transmittance vs wavelength characteristics point to an indirect bandgap of $0.6 \pm 0.5 \text{ eV}$ and significant scattering in the bulk and/or at the interface.

Keywords: VO₂ thin films; substrate biasing; transition temperature; sputtering

1. Introduction

Vanadium dioxide (VO₂) has been widely studied in recent years because of its ability to undergo a reversible metal–insulator transition (MIT) at around 68 °C, from a low-temperature insulating M-phase (monoclinic) to a high-temperature metallic R phase (rutile) [1]. This reversible transition makes VO₂ an excellent material for ultrafast optical switches, smart windows, Mott transistors, strain and gas sensors, actuators, and so forth [2–5]. The bandgap of VO₂ epitaxial films at room temperature have been reported to be about 0.7 eV [6], and would normally classify VO₂ as a semiconductor rather than an insulator, but the term “insulator” is commonly used to represent the latter semiconducting phase.

The properties of VO₂ thin films are strongly dependent on deposition processing parameters. The phase inhomogeneity in VO₂ bulk or thin films limits their potential applications by rendering the MIT phase transition broad and diffusive [3,7]. The effects of strain, grain size, stoichiometry, substrate temperature, and substrate material have been extensively studied and optimized to achieve good crystallinity with a higher optical transmittance and a higher near-IR switching contrast [8–15]. In addition to optical transmittance and switching contrast enhancement, extensive efforts have been devoted to modifying the transition temperature (T_t) of VO₂. It was reported that doping and strain control are common methods for T_t modification [16–22]. Doping elements of W, Mo, F usually decrease

the T_t [16–19], while doping elements of Al, Cr, Ti can increase the transition temperature [20,21]. The progress on T_t reduction has been successful and the T_t can be brought down by 20 °C [16]. In contrast, the studies on increasing the transition temperature of VO₂ are not many. Nevertheless, the upper bound of working temperatures for most of the electrical devices utilizing optical switches, transistors, sensors, and actuators are possibly higher than 68 °C due to the accumulated heat during service, which would result in a premature MIT of VO₂. So, a higher transition temperature of VO₂ is desirable for these applications.

In previous works, it has been found that the substrate biasing during deposition can change both the microstructure and properties of VO₂ thin films [23–25]. In this work, the effects of substrate biasing are systematically investigated with the goal of increasing the transition temperature of VO₂. We have considered only single crystal silicon substrates with the view that these VO₂ films would have to be integrated with today's silicon-based microelectronics towards hybrid optoelectronic devices. Results reported in this work show that the substrate biasing during the deposition of VO₂ thin films by DC magnetron sputtering can be effective in increasing the transition temperature.

2. Materials and Methods

Si (100) wafer substrates were ultrasonically cleaned in ethanol and dried in air for use in deposition. VO₂ thin films were deposited by DC magnetron sputtering onto Si substrates with substrate biasing (i.e., negative bias is applied to the substrate). A high-purity vanadium target (99.95%) was used and sputtered in an Argon (100 sccm) and oxygen (1.3 sccm) atmosphere at a constant pressure of 1.33 Pa and a substrate temperature of 650 °C, respectively. The applied biasing voltage ranged from 89 V to 173 V. The duration of the deposition process was 2 h with a sputtering power of 100 W.

The as-prepared VO₂ thin films were then characterized using scanning electron microscopy (SEM), Raman spectroscopy, and X-ray Photoelectron Spectroscopy (XPS). The Raman spectra were taken at room temperature using a Renishaw Invia Reflex Raman Microscope (Renishaw, Mississauga, ON, Canada). The operating laser wavelength was 514.5 nm. The optical transmission was measured in the wavelength range of 350–2500 nm using a spectrometer. The transmission measurements were carried out at 300 K (room temperature) and 368 K (above the MIT temperature). The thermal hysteresis loops were obtained by collecting transmittance values versus temperature (with 5 °C intervals both in the heating and the cooling process) at the wavelength of 2500 nm, corresponding to the largest contrast in transmittance. The XPS study was carried out using a synchrotron X-ray radiation source at the Canadian Light Source (Saskatoon, SK, Canada). The X-ray photon energy range used for this study was 5.5–250 eV and the spectra were collected using a Photoemission Scienta 100 analyzer (Scienta Omicron, Uppsala, Sweden) under ultrahigh vacuum (10^{−10} torr). The thickness of the as-deposited VO₂ thin films was measured by a Zygo Optical Profilometer (Zygo, Middlefield, OH, USA) and the grain size was determined on the SEM by using an image processing software SPIP (Version 5.1, Image Metrology, Copenhagen, Denmark).

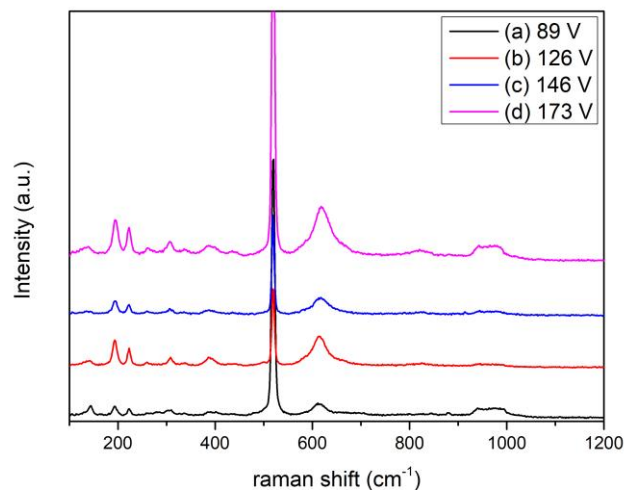
3. Results and Discussion

3.1. Microstructure Characterization by Raman

In order to study the effect of substrate biasing, we have used single-phase VO₂ thin films deposited under different substrate bias voltages. This is because nonstoichiometric VO_x thin films usually have significantly different properties compared with single-phase VO₂ and therefore cannot be used in this work. In our previous work, Raman spectroscopy results have shown to be very useful in studying the stoichiometry of VO₂ thin films [26]. Therefore, Raman measurements were again used in this study. The deposition conditions are listed in Table 1. Figure 1 shows the Raman spectra of the as-deposited VO₂ thin films. All the films show typical VO₂ with the bias voltage ranging from 89 V to 173 V, suggesting that the films have good stoichiometry [26]. The sharp Raman peak at 520 cm^{−1} and the broad peak at around 950 cm^{−1} are from the vibrations of the Si substrate [27].

Table 1. Grain size and thickness of the as-deposited VO₂ thin films with substrate biasing.

Sample #	Biasing Power (W)	Biasing Voltage (V)	Average Grain Size (nm)	Thickness (nm)
A	15	89	58.8 ± 0.6	102 ± 1
B	25	126	67.2 ± 1.0	93 ± 2
C	35	146	88.6 ± 1.2	68 ± 1
D	45	173	75.1 ± 0.5	60 ± 2

**Figure 1.** Raman spectra of the as-deposited VO₂ thin films with substrate biasing: (a) 89 V; (b) 126 V; (c) 146 V; (d) 173 V.

3.2. Surface Morphology Characterization by SEM

The surface morphology of the as-deposited VO₂ thin films was characterized by SEM and the results are shown in Figure 2. All the samples show a polycrystalline structure with a few small grains on top of large grains due to secondary nucleation. In our previous work [23], the average grain size of the VO₂ thin films deposited for 2 h (150 nm thick) without substrate biasing was 55.4 nm as shown in Figure 2e. However, the grain size of the VO₂ thin films deposited under the same conditions but with substrate biasing for 2 h (68 nm thick) was much higher and reached 88.6 nm, as shown in Table 1. Moreover, it can be seen that the deposition rate decreased with increase of substrate bias voltage, which is associated with enhanced ion bombardment. Even with reduced deposition rate and thickness, the grain size was significantly larger. This is due to the competing effects of thickness and substrate biasing. Generally, grain growth increases with increasing film thickness since grains can grow further. However, the substrate bias during deposition increases the kinetic energy of the particles impacting the coating; as a consequence, there is an increase in the surface mobility of the atoms forming the film, leading to larger crystalline grains even in thinner films. These results show that substrate biasing is very effective in grain size enlargement.

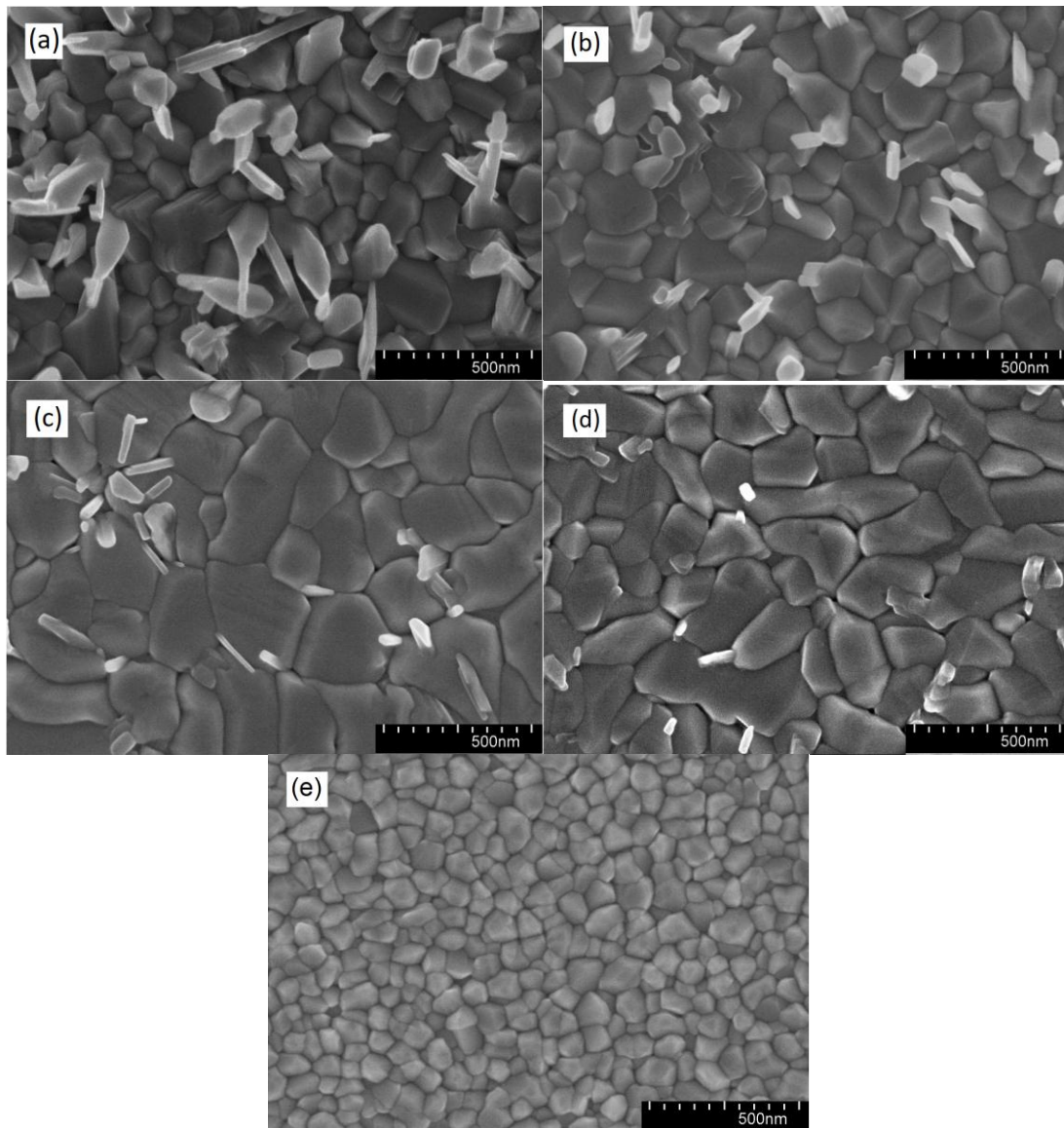


Figure 2. SEM images of VO₂ thin films deposited on Si substrates for 2 h with bias voltage of: (a) 89 V; (b) 126 V; (c) 146 V; (d) 173 V; (e) no bias on a sample prepared as in [23].

3.3. Chemical States Characterization by XPS

To fully understand the chemical states near the surface area, we have also taken x-ray photoemission spectroscopy on our as-deposited VO₂ thin films as shown in Figure 3. The measurement was performed at PGM beamline at the Canadian Light Source, with a beam size of $200 \times 200 \mu\text{m}^2$ at room temperature. We can compare the electron states of V 3d and 3p and O 2s in the films deposited under different biasing voltage in Figure 3. It should be mentioned that due to the sensitivity of this technique and the short escape depth of the electrons, the electrons accounting for the spectra are coming from the very surface, at a depth of a few Angstroms from the surface. Therefore, the spectra give information on how the V–V and V–O bonds can be distinguished from each other on the surface. Based on the XPS spectra shown in Figure 3, with all the electronic states considered, it can be concluded that the substrate biasing voltage has little influence on the V–O and V–V bonds at the surface of the thin films.

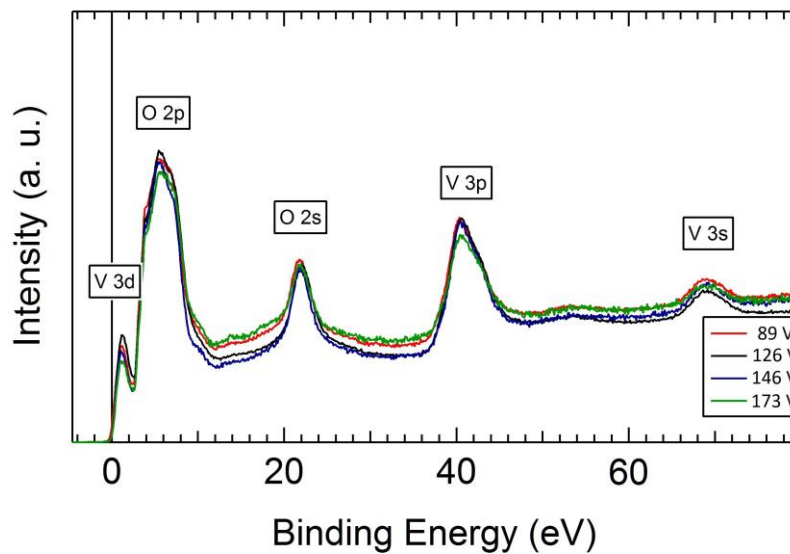


Figure 3. XPS spectra of the as-deposited VO₂ thin films with substrate biasing.

3.4. Optical Measurements

The transmission spectra of the as-deposited VO₂ thin films under different biasing conditions are shown in Figure 4. It should be noted that at wavelengths less than 1100 nm (corresponding to the 1.1 eV bandgap of Si), the Si substrate absorbs all the light as shown in Figure 4e, so there is no transmittance. The maximum transmittance reaches about 50% at a wavelength of 2500 nm. The optical transmittance of VO₂ thin films deposited under different bias voltage at (a) 300 K and (b) 368 K are shown in Figure 5. While in the insulating phase (at 300 K), the transmittance values are very close, in the metal phase (at 368 K), there is distinct dependence on the bias voltage during deposition. However, the actual effect arises from the difference in the thicknesses. The optical transmittance of a homogeneous medium generally decreases with increasing film thickness as $T = T_0 \exp(-\alpha L)$, where α is the attenuation coefficient, L is the film thickness, and the term T_0 is a pre-exponential constant (T as $L \rightarrow 0$). Figure 6 shows the semilogarithmic plots of the optical transmittance (T as %) vs the film thickness in the insulating and metal phases. The transmittance contrast ΔT (transmittance difference between normal and switched states) vs film thickness is also shown. First, consider the metal phase at 368 K, and notice the clear reduction in the transmittance as the film thickness increases, following an exponential behavior with an attenuation coefficient $\alpha \approx 3.1 \times 10^7 \text{ m}^{-1}$ at a wavelength of 2000 nm. The reason we can deduce an attenuation coefficient from the $\ln(T)$ vs L plot is that the light intensity is extinguished so much as it passes through the film in this metallic phase that interference phenomena arising from Fresnel reflections are insignificant. This is not the case in the insulating phase.

The transmittance of the VO₂/Si structure in the insulating phase at 300 K shows only a very small decrease with increasing film thickness as apparent in Figure 6. The change in T with wavelength and thickness in thin films invariably involves interference in the presence of attenuation, which is analyzed below. It should be emphasized that attenuation at 2000 nm in this phase -includes some possible band-to-band absorption and losses arises from scattering within the film as well as from any interface roughness, as discussed below.

The transmittance contrast ΔT , an important metric for device applications, increases with film thickness because of the steep decline in the transmission through the metal state.

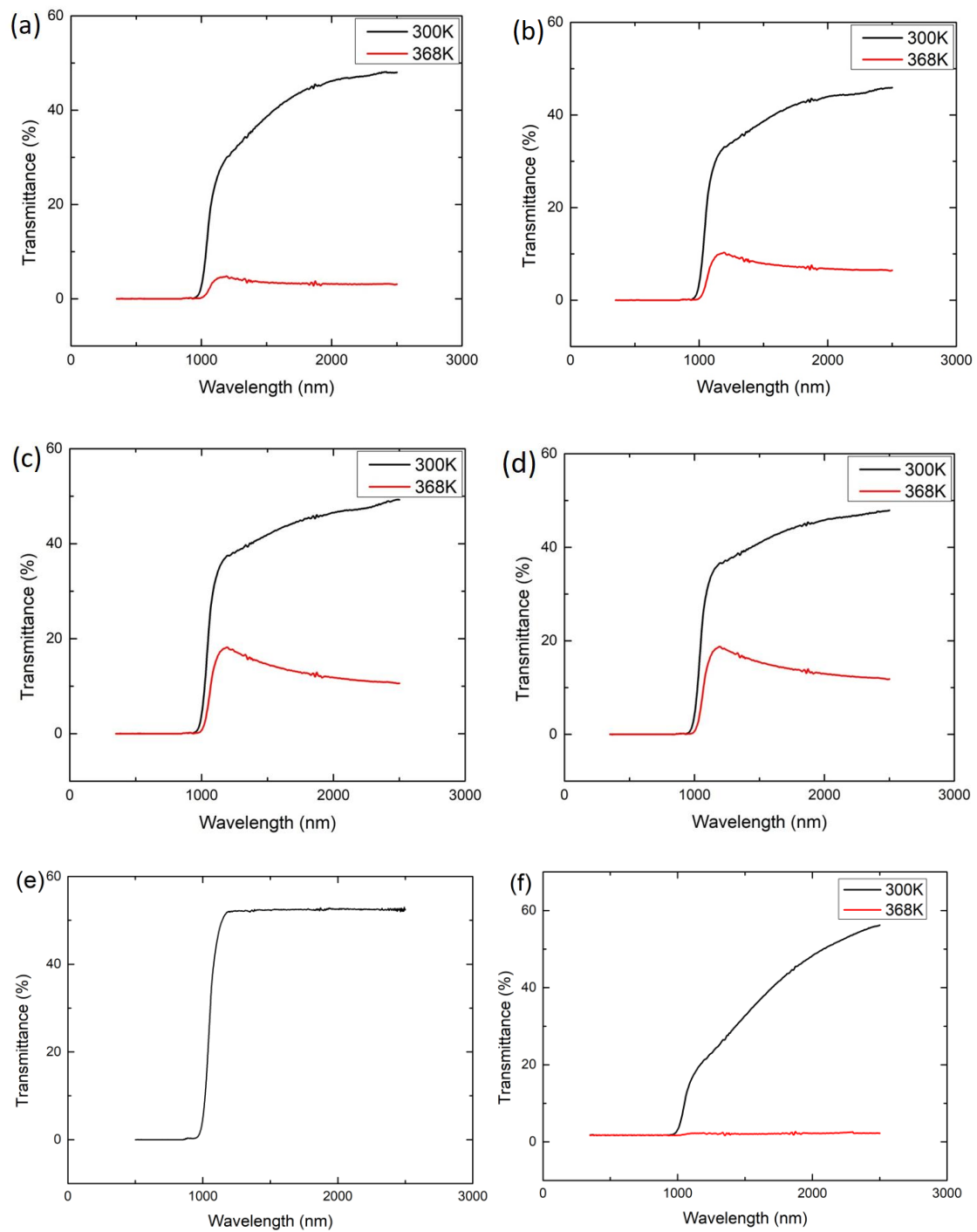


Figure 4. Optical transmittance of the as-deposited VO₂ thin films with a substrate bias voltage of: (a) 89 V; (b) 126 V; (c) 146 V; (d) 173 V; (e) bare Si substrate; (f) no bias (data extracted from reference [23] and replotted).

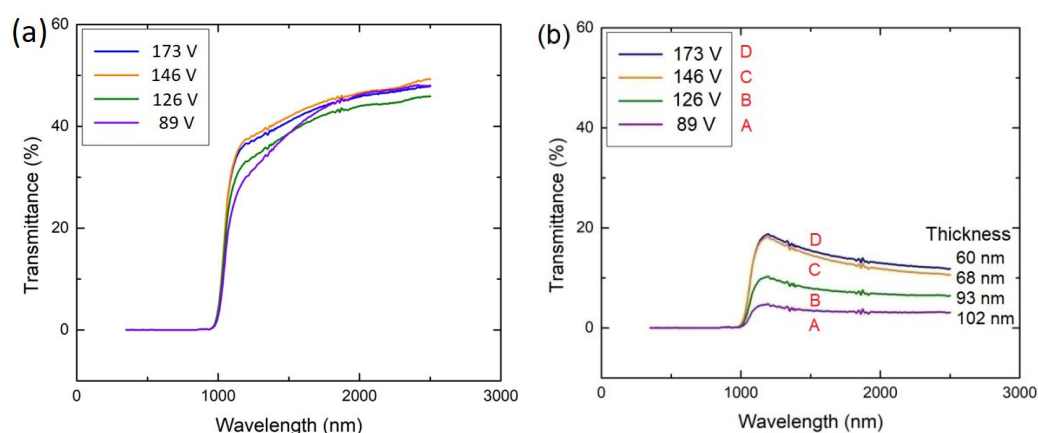


Figure 5. Optical transmittance of VO₂ thin films deposited under different bias voltage at (a) 300 K and (b) 368 K.

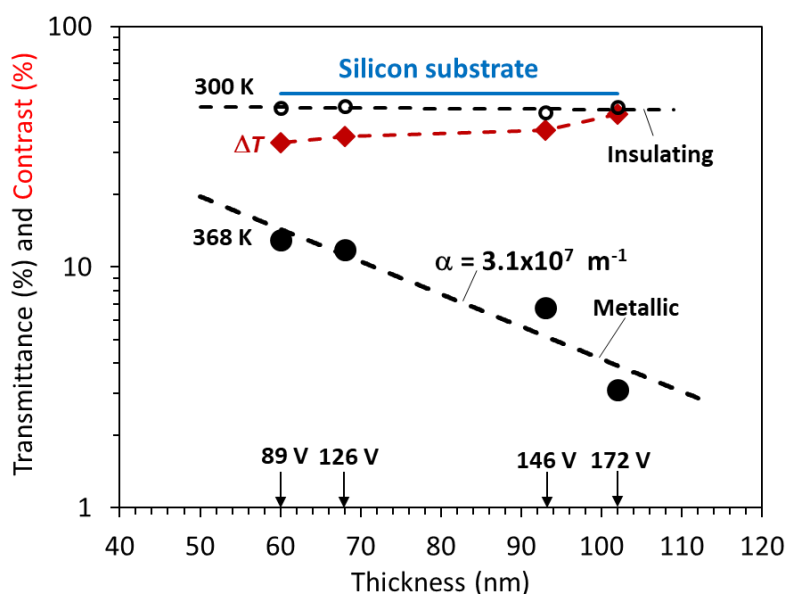


Figure 6. Optical transmittance at a wavelength of 2000 nm in the insulator and semiconductor phases (300 and 368 K, respectively) and contrast ΔT vs thickness on a semilogarithmic plot. The dashed lines are exponential fits. The attenuation coefficient of the metal phase $\alpha \approx 3.1 \times 10^7 \text{ m}^{-1}$.

Thermal hysteresis loops of transmittance vs temperature are shown in Figure 7. It can be seen that the VO₂ thin films deposited with a substrate bias voltage from 126 V to 173 V show similar hysteresis with a temperature width (ΔH) of 13 °C, while the sample deposited with 89 V bias shows a wider hysteresis with a width of 20 °C. Figure 8 provides a summary of transmittance vs temperature curves under heating and cooling schedules for all the samples; the results are generally consistent with those in Figures 4 and 5 and the implications in 6. The comparison of the hysteresis width (ΔH) of 5 °C in VO₂ thin films deposited without any bias [23], shown in Figure 7e, indicates that the VO₂ thin films deposited with biasing exhibit quite wider hysteresis loops. The ΔH widening can be attributed to grain boundaries and defects induced by the bias, and the enlarged grain size. On the other hand, the transition temperature T_t of VO₂ thin films deposited with bias increases significantly compared with those deposited without biasing. VO₂ thin films deposited without biasing show T_t of 335 K as we reported previously [23], whereas T_t of VO₂ thin films deposited with biasing reaches up to 349 K in this work. Usually the variation of the transition temperature has been associated with the stress and microstructure of the samples [28]. In this work, it is likely that the increased defect density may also lead to an increase of T_t along the lines in [29]. Another factor is the grain size. The increase of

the grain size usually leads to an increase in T_t and also the width of hysteresis ΔH as reported in [9], which is in accordance with our results. Further, the enhanced ion bombardment by biasing often generates residual stress in the as-deposited films [30]. In Figure 9, both the XRD and Raman results of VO₂ thin film deposited with biasing shows a minor shift towards higher angles or wave numbers compared with a VO₂ thin film deposited with no bias, indicating the existence of compressive stress which is induced by biasing during deposition. The significant residual stress in the films may make the phase transition harder, thus stabilizing the semiconductor phase. Therefore, the significant T_t increase (14 K) in this work could be attributed to the combined effect of enlarged grain size, increased defect density, and the residual stress induced by substrate biasing.

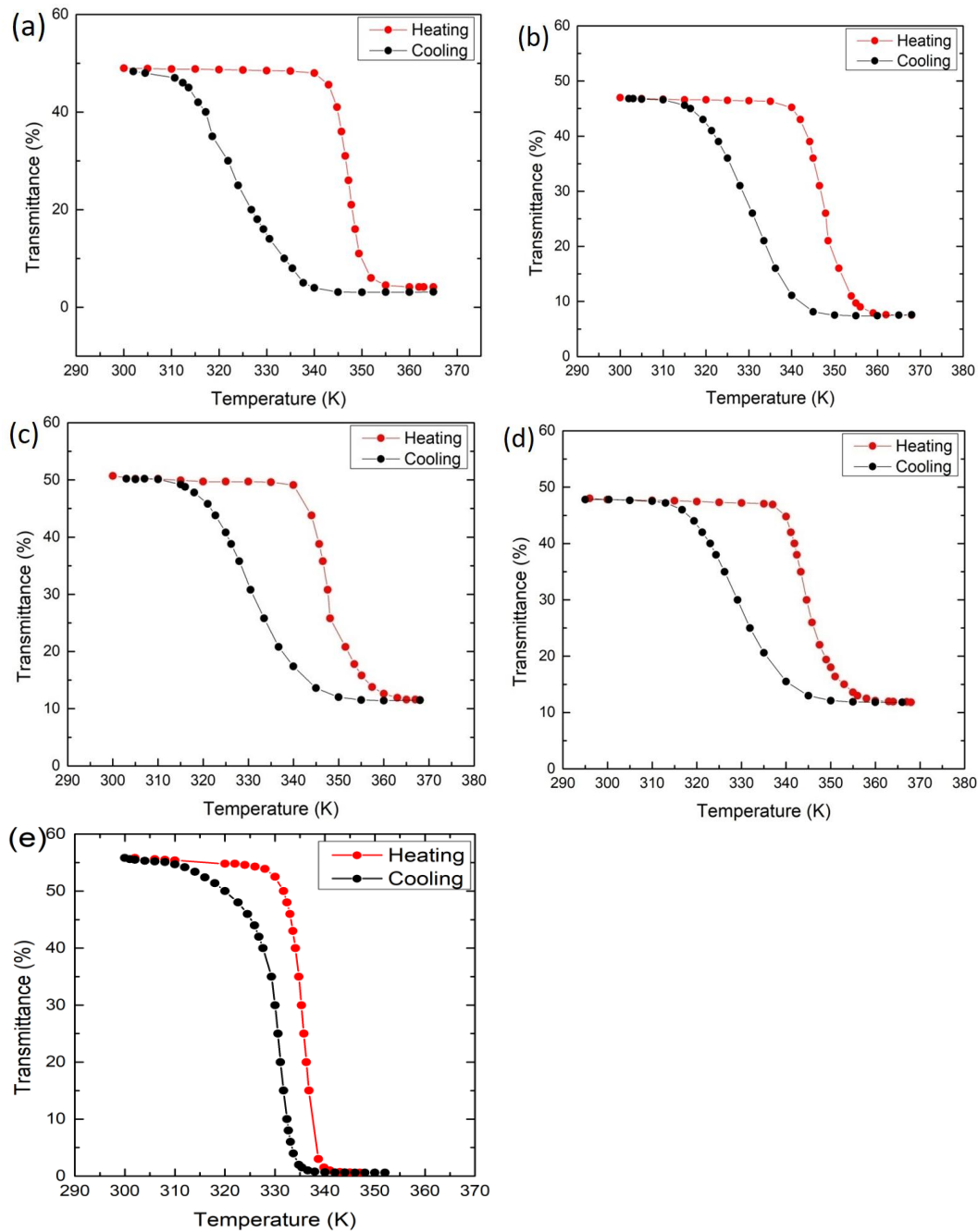


Figure 7. Optical transmittance of the as-deposited VO₂ thin films under heating (red) and cooling (black): (a) 89 V; (b) 126 V; (c) 146 V; (d) 173 V; (e) no bias (data extracted from reference [23] and replotted).

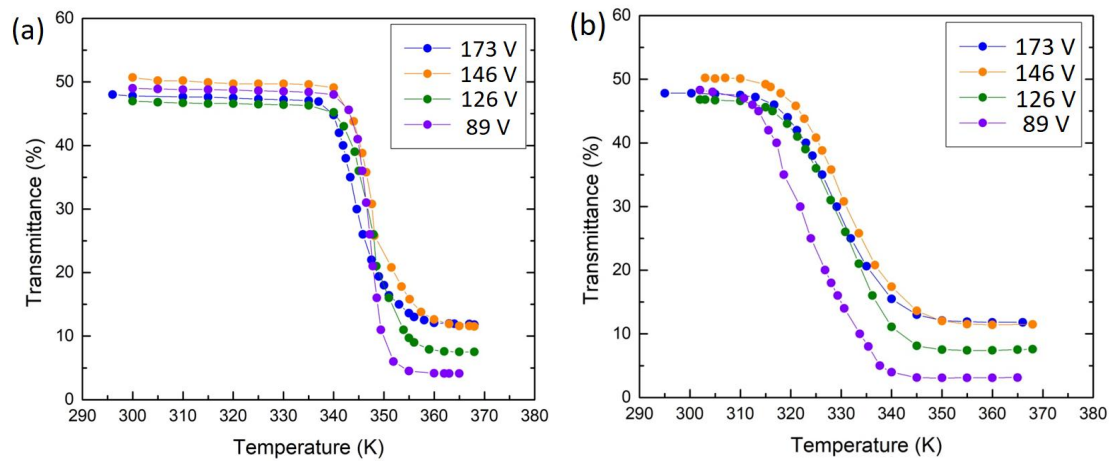


Figure 8. Optical transmittance of the as-deposited VO₂ thin films with biasing: (a) under heating and (b) under cooling.

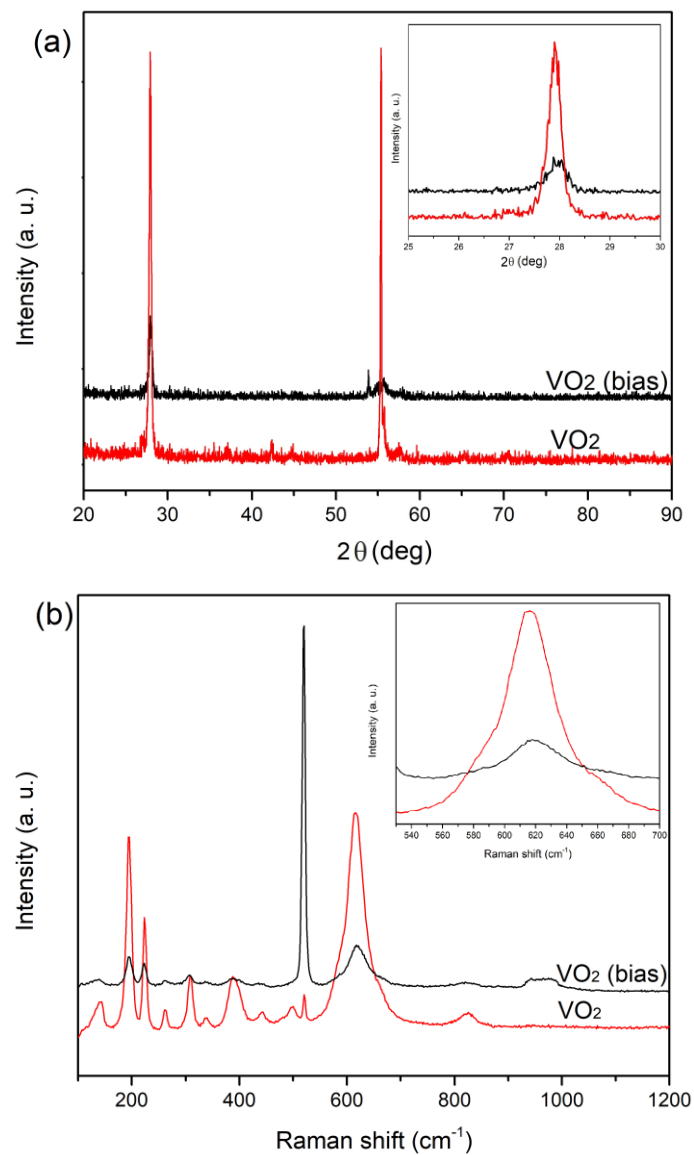


Figure 9. (a) X-ray diffraction patterns and (b) Raman spectra of VO₂ thin films (red) and VO₂ thin films deposited with 173 V bias (black).

4. Discussion

The modification of T_t of VO₂ thin films have been studied previously by others towards reducing T_t . However studies on increasing T_t of VO₂ have been only limited. In this work, the substrate biasing has been shown to be effective in increasing the T_t of VO₂. In future works, it would be useful to examine the effects of doping and strain control.

The thickness dependence of the transmittance in the metal phase in Figure 6 is very clear and leads to an attenuation coefficient of $\alpha \approx 3.1 \times 10^7 \text{ m}^{-1}$. This high attenuation coefficient represents the absorption of light and can be attributed to free carrier absorption (the Drude model) [31]

$$\alpha \approx \frac{\sigma_o}{cn\varepsilon_o(\omega\tau)^2} \quad (1)$$

where σ_o is the real part of the AC conductivity (taken as the DC conductivity), c is the speed of light, n is the refractive index, ε_o is the absolute permittivity, ω is the angular frequency ($2\pi c/\lambda$), and τ is the mean scattering time of free carriers. If μ_d is the drift mobility, then $\mu_d = e\tau/m_e^*$, where e is the elementary charge and m_e^* is the effective mass of the carriers. The measurement of the conductivity in the present case was rendered difficult due to the semiconducting silicon substrate, but typical values in the literature are $3 \times 10^4 \text{ } \Omega^{-1} \cdot \text{m}^{-1}$ for polycrystalline films [32] and $3.8 \times 10^5 \text{ } \Omega^{-1} \cdot \text{m}^{-1}$ for epitaxial films [6]. We can take a typical value of $3 \times 10^4 \text{ } \Omega^{-1} \cdot \text{m}^{-1}$ for polycrystalline films [32], as in this work, but still need τ . The drift mobility in the metallic phase is roughly $0.1 \text{ cm}^2 \cdot \text{V}^{-1} \cdot \text{s}^{-1}$ [6] and using an effective mass of $7.1m_e$, [33], we can estimate τ to be very roughly $4.0 \times 10^{-16} \text{ s}$, so that with $n \approx 2.2$ in the metal phase [34], we find the expected α to be very approximately $3.5 \times 10^7 \text{ m}^{-1}$. This is very close to the measured value, even though there were four parameters σ_o , μ_d , m_e^* , and n used from the literature. If one used an $m_e^* = 3.5m_e$ [35] instead, for example, then α is about $14 \times 10^7 \text{ m}^{-1}$, even higher. Clearly, free carrier absorption can easily account for the observed attenuation coefficient. We can also evaluate the experimental extinction coefficient K at 2000 nm from $\alpha = 2(2\pi/\lambda)K$, which gives $K \approx 4.9$.

The measured transmittance of the VO₂/Si structure in the insulating phase is obviously influenced by the substrate as well as interference of light within the film. As shown in Figure 4e, for wavelengths greater than about $\sim 1150 \text{ nm}$, the Si substrate alone is fully transparent with $T \approx 52.5\%$ with a transmittance that can be shown to be determined by the transmittance through the well-known thick plate equation (with Fresnel reflections) with $n \approx 3.50$ (e.g., [36]). The transmittance of the VO₂/Si structure, on the other hand, over the same wavelength range ($\lambda > 1150 \text{ nm}$) starts with approximately 30% and rises to about 50% as the wavelength increases from 1150 to 2500 nm. Experiments therefore point to an increase in the attenuation in the VO₂ insulating phase with decreasing wavelength, or increasing photon energy $h\nu$. We can explain the change in the transmittance T from around 1200 nm to 2500 nm by considering the transmittance of a thin film on a thick transparent substrate. Over the wavelength region where the extinction coefficient is much less than the refractive index, T can be written in terms of the Swanepoel equation [37]:

$$T = \frac{Ax}{B - Cx \cos \phi + Dx^2} \quad (2)$$

where $A = 16n^2s$, $B = (n+1)^3(n+s^2)$, $C = 2(n^2-1)(n^2-s^2)$, $D = (n-1)^3(n-s^2)$, $\phi = 4\pi nL/\lambda$, $x = \exp(-\alpha L)$ in which s is the refractive index of the substrate and α is the attenuation coefficient in the bulk of the film. We can write α as a sum of absorption and scattering contributions as

$$\alpha = \frac{A_a}{h\nu}(h\nu - E_g)^{1/m} + \frac{A_s}{\lambda^p} \quad (3)$$

where A_a a constant, E_g is the optical bandgap, and $m = 2$ for direct and $m = \frac{1}{2}$ for indirect optical transition, $h\nu$ is the photon energy ($v = c/\lambda$), A_s is a constant, and p is an index that depends on the

nature of scattering (e.g., $p = 4$ for Rayleigh scattering). Equations (2) and (3) were fitted to the data with various choices of parameters.

Figure 10 shows the experimental transmittance vs wavelength behavior from 1200 nm to 2500 nm. The colored lines are T values based on Equations (2) and (3) with $n \approx 2.8$ [38,39] and $s = 3.5$. The expected thin film transmittance with no attenuation ($\alpha = 0$) cannot explain the data, and neither can just purely band-to-band absorption with typical bandgaps of $E_g = 0.6$ eV [40,41] and 0.7 eV [6,42] with direct and indirect transitions (not shown), which means that there must be some scattering of light in the film and/or on the surfaces to account for the observed T vs λ behavior. Theoretical predictions based on Equations (2) and (3) with $E_g = 0.5$ eV to 0.7 eV and $m = \frac{1}{2}$ are shown in Figure 10 for the best-fit values of A_a , A_s , and p given in the figure caption. While $E_g = 0.6$ eV appears as a perfect fit, $E_g = 0.55$ eV is also very close. Direct transitions ($m = 2$) could not be fitted at all. Thus, we can conclude that the observed transmittance is in agreement with an indirect bandgap of 0.55–0.60 eV. The scattering index p is 2.4 but it should be remembered that any surface scattering in the present analysis based on Equations (2) and (3) would artificially inflate the scattering term and modify p . Similar good fits were found for the other samples (not shown) with values that are close to those of sample A. Table 2 summarizes the best-fit parameters for p and A_s for all the films with $E_g = 0.60$ eV and A_a kept the same for all samples; the same absorption coefficient. $A_s L$ represents the total effective scattering in the film. No unambiguous correlation could be established with grain size inasmuch as fitting a multivariable function as in the present case will invariably have uncertainties. Nonetheless, we can conclude that the insulating phase possesses an indirect bandgap of $0.60 \text{ eV} \pm 0.5 \text{ eV}$, and the films exhibit significant scattering of light.

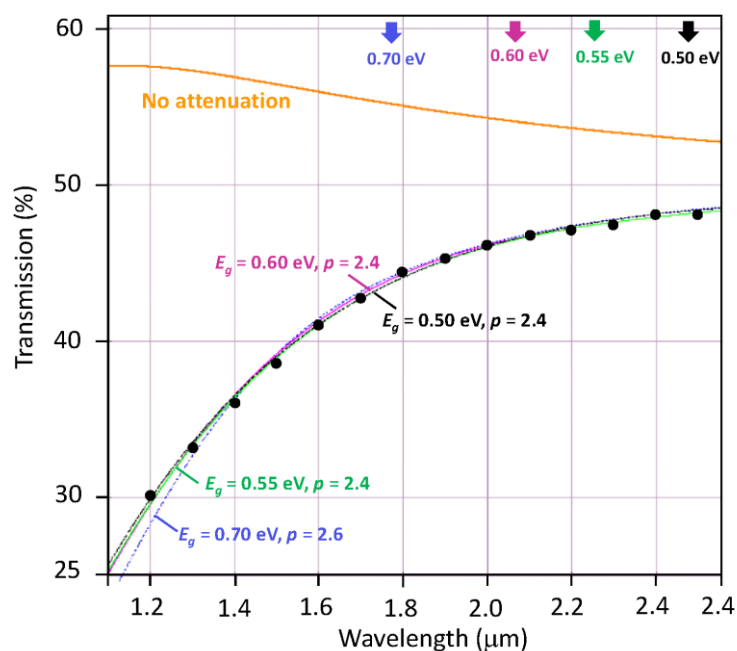


Figure 10. The transmittance vs wavelength for the 102 nm VO₂ thin film with various contributions. The orange curve is the Swanepoel transmittance with no attenuation. Other colored curves are selected fits to the data as follows: blue: $E_g = 0.70$ eV, $A_a = 0.0070 \text{ nm}^{-1} \cdot \text{eV}^{-1}$, $p = 2.6$, $A_s = 5.9 \times 10^5 \text{ nm}^{1.6}$; magenta: $E_g = 0.60$ eV, $A_a = 0.0048 \text{ nm}^{-1} \cdot \text{eV}^{-1}$, $p = 2.4$, $A_s = 1.3 \times 10^5 \text{ nm}^{1.4}$; green: $E_g = 0.55$ eV, $A_a = 0.0038 \text{ nm}^{-1} \cdot \text{eV}^{-1}$, $p = 2.4$, $A_s = 1.30 \times 10^5 \text{ nm}^{1.4}$; black: $E_g = 0.50$ eV, $A_a = 0.0035 \text{ nm}^{-1} \cdot \text{eV}^{-1}$, $p = 2.4$, $A_s = 1.25 \times 10^5 \text{ nm}^{1.4}$.

Table 2. The scattering contribution to attenuation in VO₂ films on Si, given $E_g = 0.60$ eV and $A_a = 0.0048$ nm⁻¹·eV⁻¹.

Sample #	Thickness (nm)	Average Grain Size (nm)	p	A_s (nm ^{$p-1$})	$\alpha_s L$ at 2000 nm
A	102 ± 1	58.8 ± 0.6	2.4	1.30 × 10 ⁵	0.16
B	93 ± 2	67.2 ± 1.0	1.6	4.05 × 10 ²	0.20
C	68 ± 1	88.6 ± 1.2	2.0	6.70 × 10 ³	0.11
D	60 ± 2	75.1 ± 0.5	2.2	3.65 × 10 ⁴	0.12

Finally, we can check the validity of the above arguments by noting that the strongest attenuation occurs at 1200 nm, where, using the best-fit values, the highest extinction coefficient (K) is 0.57. This is still smaller than $n = 2.8$ by a factor of 5, which provides support for the use of Equation (2) [37].

5. Conclusions

The present work clearly shows that applying substrate biasing can modify the microstructure and optical properties of VO₂ thin films deposited by magnetron sputtering. By applying substrate biasing, the deposition rate of the as-deposited VO₂ thin films decreases while the grain size increases. The films prepared under a higher bias voltage are thinner and hence show higher transmission in the metallic state. The defects induced by the substrate biasing degrade the optical properties of VO₂ in the sense that the hysteresis temperature width ΔH of the transition temperature observed during heating and cooling becomes poor. Applying substrate biasing also alters the characteristics of the phase transition. The transition temperature of VO₂ thin films deposited under bias increases 14 K accompanied by a widened hysteresis curve.

An advantage of the increased transition temperature of VO₂ thin films is the enhancement of thermal stability of VO₂ thin films for various electronic and optoelectronic device applications utilizing optical switches, transistors, sensors, and actuators, in which the working temperatures are possibly higher than 68 °C due to the accumulated heat during service.

Author Contributions: Conceptualization and formulation of ideas, C.Z., S.K., S.-J.W., R.W., and Q.Y.; methodology, X.C., M.M.; investigation, C.Z. and O.G.; writing—original draft preparation, C.Z.; writing—review and editing, Y.L., Q.Y., and S.K.; overall supervision, Q.Y. and S.K.

Funding: This research was funded jointly by NSERC (CRD) and Cisco University Research Program Fund (through Silicon Valley Community Foundation CG#602057).

Acknowledgments: The authors would like to thank Cisco Systems, and the Natural Science and Engineering Research Council of Canada (NSERC) for their financial support. The authors are also very thankful to Ramaswami Sammynaiken for the assistance in Raman and XRD testing.

Conflicts of Interest: The authors declare no conflict of interest.

References

- Morin, F.J. Oxides Which Show a Metal-to-Insulator Transition at the Neel Temperature. *Phys. Rev. Lett.* **1959**, *3*, 34–36. [[CrossRef](#)]
- Chen, S.; Ma, H.; Yi, X.; Wang, H.; Tao, X.; Chen, M.; Li, X.; Ke, C. Optical switch based on vanadium dioxide thin films. *Infrared Phys. Technol.* **2004**, *45*, 239–242. [[CrossRef](#)]
- Cheng, C.; Guo, H.; Amini, A.; Liu, K.; Fu, D.; Zou, J.; Song, H. Self-assembly and horizontal orientation growth of VO₂ nanowires. *Sci. Rep.* **2014**, *4*, 1–5. [[CrossRef](#)] [[PubMed](#)]
- Pellegrino, L.; Manca, N.; Kanki, T.; Tanaka, H.; Biasotti, M.; Bellingeri, E.; Siri, A.S.; Marré, D. Multistate memory devices based on free-standing VO₂/TiO₂ microstructures driven by Joule self-heating. *Adv. Mater.* **2012**, *24*, 2929–2934. [[CrossRef](#)] [[PubMed](#)]
- Srirodpai, O.; Wootthikanokkhan, J.; Nawalertpanya, S.; Yuwawech, K.; Meeyoo, V. Preparation, Characterization and Thermo-Chromic Properties of EVA/VO₂ Laminate Films for Smart Window Applications and Energy Efficiency in Building. *Materials* **2017**, *10*, 53. [[CrossRef](#)] [[PubMed](#)]

6. Fu, D.; Liu, K.; Tao, T.; Lo, K.; Cheng, C.; Liu, B.; Zhang, R.; Bechtel, H.A.; Wu, J. Comprehensive study of the metal-insulator transition in pulsed laser deposited epitaxial VO₂ thin films. *J. Appl. Phys.* **2013**, *113*, 043707. [[CrossRef](#)]
7. Kim, I.S.; Lauhon, L.J. Increased yield and uniformity of vanadium dioxide nanobeam growth via two-step physical vapor transport process. *Cryst. Growth Des.* **2012**, *12*, 1383–1387. [[CrossRef](#)]
8. Fan, L.L.; Chen, S.; Luo, Z.L.; Liu, Q.H.; Wu, Y.F.; Song, L.; Ji, D.X.; Wang, P.; Chu, W.S.; Gao, C.; et al. Strain dynamics of ultrathin VO₂ film grown on TiO₂(001) and the associated phase transition modulation. *Nano Lett.* **2004**, *14*, 4036–4043. [[CrossRef](#)] [[PubMed](#)]
9. Miller, M.J.; Wang, J. Influence of grain size on transition temperature of thermochromic VO₂. *J. Appl. Phys.* **2015**, *117*, 034307. [[CrossRef](#)]
10. Luo, Z.; Wu, Z.; Wang, T.; Xu, X.; Li, W.; Li, W.; Jiang, Y. Comparison of the optical responses of O-poor and O-rich thermochromic VO_x films during semiconductor-to-metal transition. *J. Phys. Chem. Solids* **2012**, *73*, 1122–1126. [[CrossRef](#)]
11. Drosos, C.; Vernardou, D. Advancements, Challenges and Prospects of Chemical Vapour Pressure at Atmospheric Pressure on Vanadium Dioxide Structures. *Materials* **2018**, *11*, 384. [[CrossRef](#)] [[PubMed](#)]
12. Chen, E.E. The influence of deposition temperature on the structure and optical properties of vanadium oxide films. *J. Vac. Sci. Technol.* **1986**, *A4*, 432–435. [[CrossRef](#)]
13. Yang, Y.; Yao, Y.; Zhang, B.; Lin, H.; Luo, Z.; Gao, C.; Zhang, C.; Kang, C. Investigating Metal-Insulator Transition and Structural Phase Transformation in the (010)-VO₂/(001)-YSZ Epitaxial Thin Films. *Materials* **2018**, *11*, 1713. [[CrossRef](#)] [[PubMed](#)]
14. Zhou, Y.; Ramanathan, S. Heteroepitaxial VO₂ thin films on GaN: Structure and metal-insulator transition characteristics. *J. Appl. Phys.* **2012**, *112*, 74114. [[CrossRef](#)]
15. Zhang, D.; Sun, H.-J.; Wang, M.-H.; Miao, L.-H.; Liu, H.-Z.; Zhang, Y.-Z.; Bian, J.-M. VO₂ Thermochromic Films on Quartz Glass Substrate Grown by RF-Plasma-Assisted Oxide Molecular Beam Epitaxy. *Materials* **2017**, *10*, 314. [[CrossRef](#)] [[PubMed](#)]
16. Fu, G.; Polity, A.; Volbers, N.; Meyer, B.K. Annealing effects on VO₂ thin films deposited by reactive sputtering. *Thin Solid Films* **2006**, *515*, 2519–2522. [[CrossRef](#)]
17. Zhu, M.-D.; Shan, C.; Li, C.; Wang, H.; Qi, H.-J.; Zhang, D.-P.; Lv, W.Z. Thermochromic and Femtosecond-Laser-Induced Damage Performance of Tungsten-Doped Vanadium Dioxide Films Prepared Using an Alloy Target. *Materials* **2018**, *11*, 1724. [[CrossRef](#)]
18. Mai, L.Q.; Hu, B.; Hu, T.; Chen, W.; Gu, E.D.; Mai, L. Electrical Property of Mo-Doped VO₂Nanowire Array Film by Melting-Quenching Sol-Gel Method. *J. Phys. Chem. B* **2006**, *110*, 19083–19086. [[CrossRef](#)]
19. Burkhardt, W.; Christmann, T.; Franke, S.; Kriegseis, W.; Meister, D.; Meyer, B.; Niessner, W.; Schallch, D.; Scharmann, A. Tungsten and fluorine co-doping of VO₂ films. *Thin Solid Films* **2002**, *402*, 226–231. [[CrossRef](#)]
20. Bêteille, F.; Livage, J. Optical Switching in VO₂ Thin Films. *J. Sol-Gel Sci. Technol.* **1998**, *13*, 915–921. [[CrossRef](#)]
21. Du, J.; Gao, Y.; Luo, H.; Kang, L.; Zhang, Z.; Chen, Z.; Cao, C. Significant changes in phase-transition hysteresis for Ti-doped VO₂ films prepared by polymer-assisted deposition. *Sol. Energy Mater. Sol. Cells* **2011**, *95*, 469–475. [[CrossRef](#)]
22. Liu, M.K.; Wagner, M.; Abreu, E.; Kittiwatanakul, S.; McLeod, A.; Fei, Z.; Goldflam, M.; Dai, S.; Fogler, M.; Lu, J.; et al. Anisotropic Electronic State via Spontaneous Phase Separation in Strained Vanadium Dioxide Films. *Phys. Rev. Lett.* **2013**, *111*, 096602. [[CrossRef](#)] [[PubMed](#)]
23. Zhang, C.; Koughia, C.; Li, Y.; Cui, X.; Ye, F.; Shiri, S.; Sanayei, M.; Wen, S.-J.; Yang, Q.; Kasap, S. Near-zero IR transmission of VO₂ thin films deposited on Si substrate. *Appl. Surf. Sci.* **2018**, *440*, 415–420. [[CrossRef](#)]
24. Bobyak, L.; Fallon, P.; Razavi, A. The effects of biasing and annealing on the optical properties of radio-frequency sputtered VO₂. *J. Vac. Sci. Technol. A* **1990**, *8*, 1391–1394.
25. Azhan, N.H.; Okimura, K.; Ohtsubo, Y.; Kimura, S.-I.; Zaghrioui, M.; Sakai, J. Large modification in insulator-metal transition of VO₂ films grown on Al₂O₃ (001) by high energy ion irradiation in biased reactive sputtering. *J. Appl. Phys.* **2016**, *119*, 055308. [[CrossRef](#)]
26. Zhang, C.; Yang, Q.; Koughia, C.; Ye, F.; Sanayei, M.; Wen, S.-J.; Kasap, S. Characterization of vanadium oxide thin films with different stoichiometry using Raman spectroscopy. *Thin Solid Films* **2016**, *620*, 64–69. [[CrossRef](#)]
27. Li, B.; Yu, D.; Zhang, S.-L. Raman spectral study of silicon nanowires. *Phys. Rev. B* **1999**, *59*, 1645–1648. [[CrossRef](#)]

28. De Natale, J.F.; Hood, P.J.; Harker, A.B. Formation and characterization of grain-oriented VO₂ thin films. *J. Appl. Phys.* **1989**, *66*, 5844–5850. [[CrossRef](#)]
29. Mihailescu, C.N.; Symeou, E.; Svoukis, E.; Negrea, R.F.; Ghica, C.; Teodorescu, V.S.; Tanase, L.C.; Negrilă, C.; Giapintzakis, J. Ambiguous Role of Growth-Induced Defects on the Semiconductor-to-Metal Characteristics in Epitaxial VO₂/TiO₂ Thin Films. *ACS Appl. Mater. Interfaces* **2018**, *10*, 14132–14144. [[CrossRef](#)]
30. Bull, S.J.; Jones, A.M.; MacCabe, A.R. Residual stress in ion-assisted coatings. *Surf. Coat. Technol.* **1992**, *54/55*, 173–179. [[CrossRef](#)]
31. Kasap, S.O. *Principles of Electronic Materials and Devices*, 4th ed.; McGraw-Hill: New York, NY, USA, 2018; p. 896.
32. Chain, E.A. Optical properties of vanadium dioxide and vanadium pentoxide thin films. *Appl. Opt.* **1991**, *30*, 2782. [[CrossRef](#)] [[PubMed](#)]
33. Rosevear, W.H.; Paul, W. Hall effect in VO₂ near the Semiconductor-To-Metal transition. *Phys. Rev. B* **1973**, *7*, 2109. [[CrossRef](#)]
34. Kivaisi, R.; Samiji, M. Optical and electrical properties of vanadium dioxide films prepared under optimized RF sputtering conditions. *Sol. Energy Mater. Sol. Cells* **1999**, *57*, 141–152. [[CrossRef](#)]
35. Hensler, D.H. Transport Properties of Sputtered Vanadium Dioxide Thin Films. *J. Appl. Phys.* **1968**, *39*, 2354. [[CrossRef](#)]
36. Kasap, S.O. *Optoelectronics and Photonics: Principles and Practices*, 2nd ed.; Pearson: Upper Saddle River, NJ, USA, 2013; p. 73.
37. Swanepoel, R. Determination of the thickness and optical constants of amorphous silicon. *J. Phys. E Sci. Instrum.* **1983**, *16*, 1214–1222. [[CrossRef](#)]
38. Wan, C.; Zhang, Z.; Woolf, D.; Hessel, C.M.; Rensberg, J.; Hensley, J.M.; Xiao, Y.; Shahsafi, A.; Salman, J.; Richter, S.; et al. Optical properties of thin-film vanadium oxide from the visible to the far infrared. *arXiv preprint* **2019**.
39. Swann, J.T.; De Smet, D.J. Ellipsometric investigation of vanadium dioxide films. *J. Appl. Phys.* **1985**, *58*, 1335–1338. [[CrossRef](#)]
40. Parker, J.C.; Geiser, U.W.; lam, D.J.; Xu, Y.; Ching, W.Y. Optical properties of the vanadium oxides VO₂ and V₂O₅. *J. Am. Ceram. Soc.* **1990**, *73*, 3206–3208. [[CrossRef](#)]
41. Lin, T.; Wang, J.; Liu, G.; Wang, L.; Wang, X.; Zhang, Y. Influence of Discharge Current on Phase Transition Properties of High Quality Polycrystalline VO₂ Thin Film Fabricated by HiPIMS. *Materials* **2017**, *10*, 633. [[CrossRef](#)]
42. Shin, S.; Suga, S.; Taniguchi, M.; Fujisawa, M.; Kanzaki, H.; Fujimori, A.; Daimon, H.; Ueda, Y.; Kosuge, K.; Kachi, S. Vacuum-ultraviolet reflectance and photoemission study of the metal-insulator phase transitions in VO₂, V₆O₁₃, and V₂O₃. *Phys. Rev. B Condens. Matter* **1990**, *41*, 4993–5009. [[CrossRef](#)]

